JOURNAL OF THERMOPHYSICS AND HEAT TRANSFER
Vol. 21, No. 1, January–March 2007

Heat Transfer in Loop Heat Pipes Capillary Wick: Effect Effective Thermal Conductivity

Chuan Ren* and Qing-Song Wu†
University of Science and Technology of China, 230026 Hefei, Anhui, People's Republic of China

DOI: 10.2514/1.23599

An axisymmetric two-dimensional mathematical model of the cylindrical evaporator's wick of loop heat pipes is developed to simulate heat transfer with flow and evaporation in the capillary porous structure. The effect of the interaction between the flowfield and the liquid–vapor interface on the position of the interface and the curvature of menisci is adequately considered in this model. The results obtained in this paper are reasonable and agree with experimental results in the literature. The effect of the wick's effective thermal conductivity on the loop heat pipe's performance is investigated in detail. It has little influence on the driving performance but affects strongly the heat transfer performance.

Nomenclature

A_s	=	area of a close-contacted heated fin
c	=	special thermal capacity, J/(kg · K)
h	=	enthalpy, J/kg
K	=	permeability, m^2
k	=	thermal conductivity, W/(m · K)
$\dot{m}$	=	flux of the working fluid, kg/s
$\boldsymbol{n}$	=	normal vector at liquid–vapor interface
p	=	pressure, Pa
q	=	heat flux, W/m^2
R	=	radius of menisci's curvature, m
R_M	=	gas constant, J/(kg · K)
$\boldsymbol{r}$	=	position vector of meniscus, m
$\boldsymbol{s}$	=	displacement vector of interface, m
T	=	temperature, K
t	=	time, s
U	=	total heat transfer coefficient, W/(m^2 · K)
$\boldsymbol{V}$	=	velocity vector of infiltration, m/s

Greek symbols

β_p	=	expansion coefficient with constant temperature, 1/Pa
β_T	=	expansion coefficient with constant pressure, 1/K
λ	=	latent heat of evaporation, J/kg
μ	=	dynamic viscosity, kg/(m · s)
ν	=	kinematic viscosity, m^2/s
ρ	=	density, kg/m^3
σ	=	coefficient of surface tension, N/m
ϕ	=	porosity

Subscripts

c	=	capillary
e	=	reference
eva	=	evaporation
exit	=	on the exit
f	=	fluid
g	=	vapor
in	=	on the entrance
l	=	liquid
n	=	normal direction
out	=	on the exit
r	=	on radial direction
s	=	saturated
t	=	total
wall	=	on the heated wall
z	=	on longitudinal direction

Received 3 March 2006; revision received 15 April 2006; accepted for publication 19 May 2006.

*Doctor, Department of Thermal Science and Energy Engineering.
†Professor, Department of Thermal Science and Energy Engineering; qswu@ustc.edu.cn. Corresponding author.

Introduction

THE loop heat pipe (LHP) is a two-phase thermal control device with the capillary pump driving a working fluid to flow and transfer heat over a large distance, just as the capillary pumped loop (CPL). As their growing application to many engineering domains including thermal management of satellites and spacecrafts as well as cooling of electrical and electronic devices, research into CPLs and LHPs has become active and important in the last decade [1–9]. Kaya and Hoang [1,2] simulated the steady-state performance of a LHP by a mathematical model based on the steady-state energy conservation and the pressure drop calculations along the fluid path, and the experimental validation was carried out. Hoang and Ku [3] researched hydrodynamic aspects of CPLs, Ku [4] investigated operating characteristics of LHPs, Pouzet et al. [6] investigated dynamic response of a CPL at various heat loads, and Zhang et al. [9] focused on the startup behavior of a LHP. Vasiliev [7] and Maydanik [8] reviewed the research of LHPs in 2005. Most of the previous research focused on tests or simulations of the whole device; many important properties of evaporators were neglected. The evaporator with the capillary porous structure is the primary functional component that accepts heat fluxes, organizes evaporation, and produces the driving force of the working fluid flowing circularly in the whole device. Heat transfer with coupled flow and evaporation occurs just in the capillary porous structure, and so it is important and necessary to investigate the dynamic and thermodynamic behavior of the working fluid in the capillary porous structure.

Generally, the wick's performances are evaluated from three aspects: the driving performance, the heat transfer performance, and the capillary effect of evaporation. The driving performance is related to the flow of the working fluids and the heat transfer limit. The heat transfer performance evaluates the LHP's heat transfer efficiency. The capillary effect of evaporation is related to the difficulty of organizing evaporation in the capillary porous structure. Besides heat flux, the wick's working state and performances are influenced by many factors. Although it is attractive for researchers and engineers to understand each effect on the wick's working state and performances, it is difficult to realize separately the research to each effect through experiments. For example, the effect of effective thermal conductivity is often mixed with the effect of permeability in

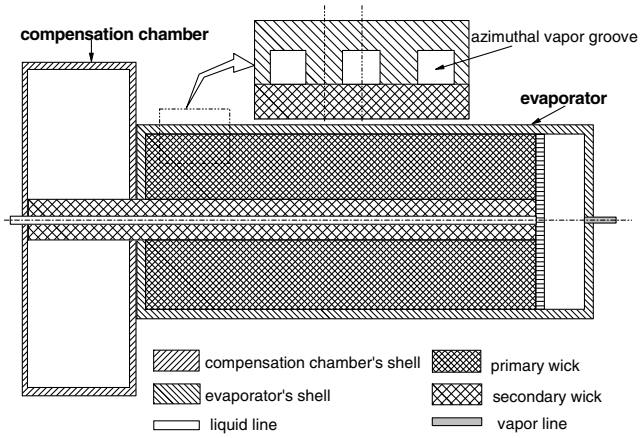

Fig. 1 Configuration of the evaporator with azimuthal grooves and the compensation chamber.

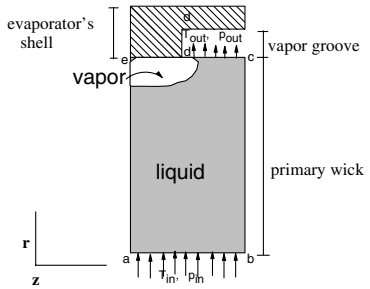

Fig. 2 Diagram of the cell for simulation with width of half-tooth and half-groove.

experiments due to their relation to the wick's structure. Whereas it can be realized in numerical simulation to research each effect separately.

In this paper, an axisymmetric two-dimensional mathematical model of the cylindrical evaporator's wick with azimuthal vapor grooves of LHPs is developed. The effect of the interaction between the flowfield and the liquid–vapor interface on the position of the interface and the curvature of menisci is adequately considered in this model. The effect of the wick's effective thermal conductivity on the LHP's performances is investigated in detail.

Mathematical Model and Numerical Simulation

Different from the conventional cylindrical evaporators of LHPs, the evaporator of 16 mm in diameter, investigated in this paper, has the primary wick, the secondary wick, eight deeper longitudinal grooves, and plenty of shallower azimuthal grooves in its shell wall. The configuration is illustrated in Fig. 1. The primary wick is 5 mm thick in the radial direction, and it is made of sintered nickel powders with an effective pore radius of 0.001 mm and porosity of 0.5. The width of the azimuthal groove is 1 mm, as is the width of a heated fin. In our simulation, a cell shown in Fig. 2 is used to represent the entire primary wick because of the periodic heated boundary on the top and the geometrical and physical symmetry. It is 5 mm thick in the radial direction and 1 mm wide in the longitudinal direction.

Some assumptions are introduced:

1) There is homogeneous, isotropic and rigid capillary porous media; the fluids are slightly compressible.

2) The properties for the solid, liquid, and vapor are constant.

3) Gravity, heat radiation, and viscous dissipation are neglected; there is no inner heated source.

4) There is axisymmetric flow to the evaporator's axis and no flow in the azimuthal direction.

5) Local thermal equilibrium exists between the solid and fluid phases.

6) Evaporation occurs on the liquid–vapor interface; no boiling occurs in liquid.

The continuum equation of fluid in porous media is as follows:

$$\frac{\partial}{\partial t}(\rho_f \phi) + \nabla \cdot (\rho_f \boldsymbol{V}) = 0 \tag{1}$$

Replacing the momentum equation of fluid in porous media, Darcy's law is presented with gravity neglected:

$$\boldsymbol{V} = -\frac{K}{\mu}\nabla p \tag{2}$$

The equation of state is derived as follows:

$$\rho_f = \rho_{o,f}[1 - \beta_{T,f}(T - T_e) + \beta_{p,f}(p - p_e)], \qquad f = l, g \tag{3}$$

Combining Eq. (1) with Eqs. (2) and (3), the pressure equation in cylindrical polar coordinates is derived as

$$\frac{\phi}{K}\frac{\partial}{\partial t}[\rho_{0,f}\beta_{p,f}(p - p_e)] - \frac{1}{r}\frac{\partial}{\partial r}\left(\frac{r}{\nu_f}\frac{\partial p}{\partial r}\right) - \frac{\partial}{\partial z}\left(\frac{1}{\nu_f}\frac{\partial p}{\partial z}\right) = -\frac{\phi}{K}\frac{\partial}{\partial t}\{\rho_{0,f}[1 - \beta_{T,f}(T - T_e)]\} \tag{4}$$

where ν_f is the kinematic viscosity.

According to the assumptions, the enthalpy equation for coupled solid and fluid phases in cylindrical polar coordinates is derived as

$$\frac{\partial}{\partial t}(\rho_t h_f) + \frac{1}{r}\frac{\partial}{\partial r}(r\rho_f V_r h_f) + \frac{\partial}{\partial z}(\rho_f V_z h_f) = \phi\frac{\partial p}{\partial t} + V_r\frac{\partial p}{\partial r} + V_z\frac{\partial p}{\partial z} + \frac{1}{r}\frac{\partial}{\partial r}\left[rk_t\frac{\partial}{\partial r}\left(\frac{h_f - h_{0,f}}{c_{p,f}}\right)\right] + \frac{\partial}{\partial z}\left[k_t\frac{\partial}{\partial z}\left(\frac{h_f - h_{0,f}}{c_{p,f}}\right)\right] \tag{5}$$

where V_r and V_z are the velocity of infiltration in the radial and longitudinal directions, respectively.

$$\rho_t \equiv \phi\rho_f + (1 - \phi)\rho_s\frac{c_s}{c_{p,f}} \tag{6}$$

$$h_f = h_{0,f} + c_{p,f}(T - T_e) \tag{7}$$

The boundary conditions with L_r and L_z standing for the radial thickness and the longitudinal width of a cell, respectively, are listed in the following. The saturated liquid lies on the entrance with the temperature $T_{\text{in}} = 293$ K and the pressure $P_{\text{in}} = 882,500$ Pa.

1) When $z = 0$ or $z = L_z$ (the boundaries b–c and a–e in Fig. 2),

$$\frac{\partial T}{\partial z} = 0, \qquad \frac{\partial p}{\partial z} = 0 \tag{8a}$$

2) When $r = r_{\text{in}}$ (the boundary a–b in Fig. 2),

$$T = T_{\text{in}}, \qquad p = p_{\text{in}} \tag{8b}$$

3) When $r = r_{\text{out}} = r_{\text{in}} + L_r$ and $0 < z < L_z/2$ (the boundary d–e in Fig. 2),

$$\begin{cases} \frac{\partial p}{\partial r} = 0, & \text{if the interface doesn't lie on the boundary d–e} \\ -\rho_f\frac{K}{\mu_f}\frac{\partial p}{\partial r}\Big|_l \lambda = q - k_t\frac{\partial T}{\partial r}\Big|_l, & \text{if the interface lies on the boundary d–e} \end{cases} \tag{8c}$$

and

$$\begin{cases} -k_t \frac{\partial T}{\partial r} = q, & \text{if the interface doesn't lie on the boundary d–e} \\ -k_t \frac{\partial T}{\partial r}\Big|_g = q, & \text{if the interface lies on the boundary d–e} \end{cases} \tag{8d}$$

4) When $r = r_{\text{out}} = r_{\text{in}} + L_r$ and $L_z/2 < z < L_z$ (the boundary c–d in Fig. 2),

$$\begin{cases} p = p_{\text{out}}, & \text{if the interface doesn't lie on the boundary d–e} \\ -\rho_f \frac{K}{\mu_f} \frac{\partial p}{\partial r}\Big|_l \lambda = k_t \frac{\partial T}{\partial r}\Big|_l, & \text{if the interface lies on the boundary d–e} \end{cases} \tag{8e}$$

and

$$\begin{cases} \frac{\partial T}{\partial r} = 0, & \text{if the interface doesn't lie on the boundary d–e} \\ \frac{\partial T}{\partial r}\Big|_g = 0, & \text{if the interface lies on the boundary d–e} \end{cases} \tag{8f}$$

Before startup, pressure and temperature are homogeneous in the full liquid-saturated porous medium, and the working fluid is saturated and resting.

The conservation and jump of the variants on the liquid–vapor interface in capillary porous media is listed next.

$$T_g|_{s(r,t)} = T_l|_{s(r,t)} \tag{9a}$$

$$p_g|_{s(r,t)} - p_l|_{s(r,t)} = \frac{2\sigma}{R(\boldsymbol{r}, t)} \tag{9b}$$

$$\rho_g \left(\phi \frac{\mathrm{d}\boldsymbol{s}(\boldsymbol{r}, t)}{\mathrm{d}t} - \boldsymbol{V}_g \right) \cdot \boldsymbol{n} = \rho_l \left(\phi \frac{\mathrm{d}\boldsymbol{s}(\boldsymbol{r}, t)}{\mathrm{d}t} - \boldsymbol{V}_l \right) \cdot \boldsymbol{n} \tag{9c}$$

$$\begin{aligned} &\rho_g h_g \left(\phi \frac{\mathrm{d}\boldsymbol{s}(\boldsymbol{r}, t)}{\mathrm{d}t} - \boldsymbol{V}_g \right) \cdot \boldsymbol{n} + \left(k_t \frac{\partial T}{\partial n} \right)_g \\ &\quad = \rho_l h_l \left(\phi \frac{\mathrm{d}\boldsymbol{s}(\boldsymbol{r}, t)}{\mathrm{d}t} - \boldsymbol{V}_l \right) \cdot \boldsymbol{n} + \left(k_t \frac{\partial T}{\partial n} \right)_l \end{aligned} \tag{9d}$$

where $\boldsymbol{s}(\boldsymbol{r}, t)$ and $\mathrm{d}\boldsymbol{s}(\boldsymbol{r}, t)/\mathrm{d}t$ are the displacement and velocity of the interface and $R(\boldsymbol{r}, t)$ is the radius of menisci's curvature, respectively.

The capillary force is presented in the Kelvin equation:

$$p_g = p_s(T) \exp\left(-\frac{p_c}{\rho_l R_M T} \right) \tag{10}$$

where R_M is the gas constant for ammonia. $p_s(T)$ is determined by the Clausius–Clapeyron equation:

$$p_s(T) = p_e \exp\left[\frac{\lambda}{R_M} \left(\frac{1}{T_e} - \frac{1}{T} \right) \right] \tag{11}$$

By using (9d), the velocity and displacement of the interface follow.

$$\frac{\mathrm{d}s_n}{\mathrm{d}t} = \frac{(\rho_l h_l V_{n,l} - \rho_g h_g V_{n,g}) - [k_{t,l}(\partial T/\partial n)|_l - k_{t,g}(\partial T/\partial n)|_g]}{\phi(\rho_l h_l - \rho_g h_g)} \tag{12}$$

$$s_n = s_n^0 + \frac{\mathrm{d}s_n}{\mathrm{d}t} \cdot \Delta t \tag{13}$$

In this model, a staggered background mesh of 100×20 with a local thin grid in the radial direction is introduced. The number of local thin grids in a background grid is determined not by the possible position of the liquid–vapor interface but by the gradient of temperature near the heated fin, which is greater at higher heat flux and requests more thin grids in a background grid. The finite volume method is introduced to discretize the pressure Eq. (4) and the enthalpy Eq. (5), respectively, in the liquid and vapor region whereas the boundary conditions are treated as in [10]. The capillary force is treated as the inner boundary on the basis of Eq. (9b). The discretized Eqs. (4) and (5) are treated separately by the strong implicit procedure [10] and are coupled together in every time step whereas an explicit front tracking method with (12) and (13) is used. The steady state is reached when the maximum relative change of both pressure and temperature among continuous transient states is less than 10^{-6}.

Results and Discussions

General Simulation

The patterns of steady flowfields at different heat fluxes are similar qualitatively, but there are differences in the magnitude. An example at $q = 20,000\ \mathrm{W/m^2}$ is presented in Figs. 3 and 4. Pressure decreases gradually along the radial direction from the entrance to the interface and jumps up suddenly on the interface. Discontinuous pressure on the interface indicates the capillary force, which is the driving force of a LHP. There lies a steady vapor blanket between the liquid-saturated zone in the porous media and the close-touched heated fins for a definite interval of heat fluxes [11], but vapor blankets at low or moderate heat fluxes are too thin to be observed in experiments [12]. Our results agree with those of [11,12]. As results of the field of pressure, fluid flows fully in the radial direction in most regions of the wick whereas two-dimensional flow occurs only in the vicinity of heated fins and grooves. The radial velocity decreases along the radial direction in most regions due to the flowing area enlarging along the radial direction, and it increases in the vicinity of heated fins because the effect of evaporation is stronger than the effect of the flowing area.

As shown in Fig. 3b, temperature increases along the radial direction from the entrance to heated fins, and there are two-dimensional patterns of isotherms in the vicinity of heated fins and grooves. For a metal wick with high thermal conductivity, its metal framework constitutes a channel net of heat flow that diffuses heat around from the heat source. Evaporation occurs everywhere on the liquid–vapor interface in the porous media including the section far from the heat source where evaporating energy is local heat. The results are coincident to those of [13] but different from those of [14,15], which assumed that no evaporation occurred on the interface between the vapor groove and the liquid-saturated wick. As shown in Fig. 4, temperature rises slightly along the boundary c–d where the region with scarce heat support lies. The profile of temperature has a steep slope at spot d, which indicates that a thin vapor blanket lies between the heated fin and the liquid-saturated zone in the porous media. The distribution of radial velocities on the interface indicates the intensity of evaporation. The closer the region is to the center of the heat source, the more intensely it is vaporizing.

The variation of mean temperatures on the heat fin and on the exit versus the time after startup at different heat fluxes are shown in Fig. 5. The magnitude of temperature increases as heat flux increases.

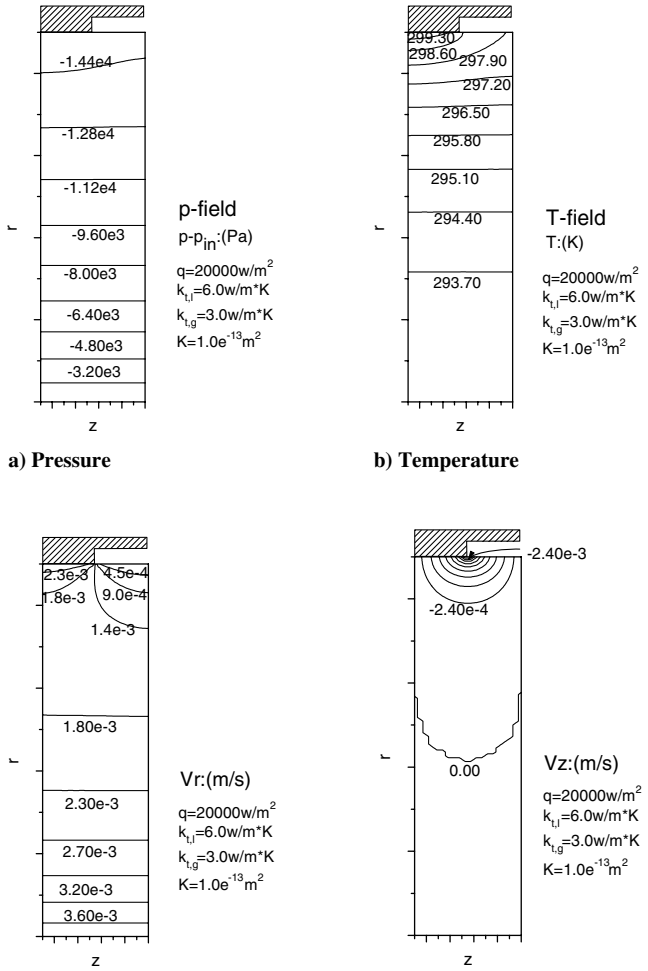

a) Pressure b) Temperature

c) Radial velocity d) Longitudinal velocity

Fig. 3 Isogram of steady state (the radial thickness 5 mm and the longitudinal width 1 mm).

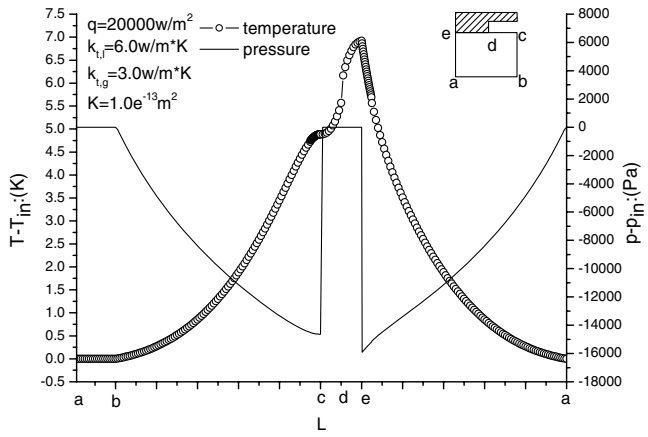

Fig. 4 Profiles of pressure and temperature along the boundary of steady state.

The temperature difference between the heated fin and the exit changes little when it approaches steady state. With a log scale on the time axis, one can see that the variation of temperature becomes smaller and smaller with time. These results validate the celerity of the LHP's startup.

Effect of Wick's Effective Thermal Conductivity on Loop Heat Pipe's Performance

Inside granule-packed or sintered porous media there are netlike channels that diffuse fluid and heat in all directions. The effective

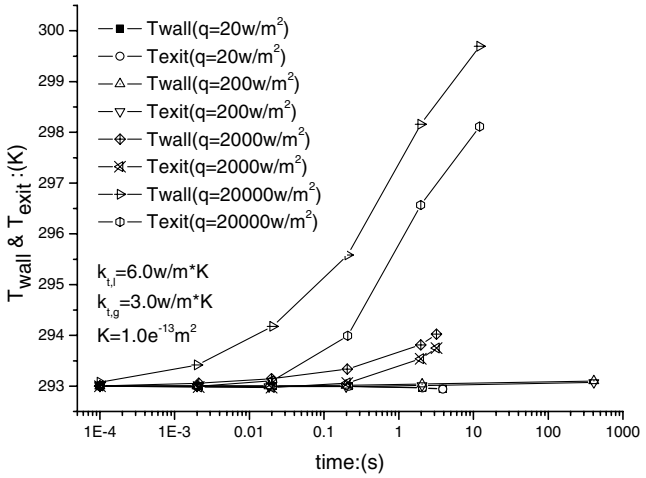

Fig. 5 Variation of mean temperatures T_{wall} and T_{exit} versus time after startup at different heat fluxes.

thermal conductivity depends on not only the properties of the working fluid and solid framework but also the structure of the porous media. Because of its diversity, there is no universal formula suitable for every porous medium so far. In this paper, the fiducial effective thermal conductivity, $k_{t,l} = 6.0\ \text{W/m} \cdot \text{K}$, is the experimental result of a nickel-sintered capillary wick filled with liquid saturating ammonia. And the effective thermal conductivity of the dry wick, $k_{t,g}$, is half of it. In this section, we simulate the effect of effective thermal conductivity on the wick's performance. The change of effective thermal conductivity can be realized by replacing the material that constructs the solid framework while the structure of porous media remains.

The LHP is a self-driving device depending on heat flux. Heat flux leads to evaporation of the working fluid, and the capillary force at menisci that are formed by evaporation of the working fluid in the porous media drives the working fluid flowing. Therefore, compared with other effects, heat flux determines primarily the magnitude of pressure and temperature. During heat transfer with flow and evaporation in the LHP's wick, there are three competing dynamic and thermodynamic processes: evaporation, heat conduction of the porous structure, and convection of the cool working liquid, among which evaporation occurs only on the interface. The combined effect of the three processes determines pressure, temperature, the position of the interface, the curvature of menisci, and so on.

Heat flux obeys the following balance of energy

$$qA_s = \dot{m}[c_{p,l}(T_{\text{eva}} - T_{\text{in}}) + \lambda + c_{p,g}(T_{\text{exit}} - T_{\text{eva}})] \qquad (14)$$

In (14), the two terms in the square brackets are called sensible heat. Combining Eqs. (2) and (14), considering sensible heat much smaller than latent heat, we predict that the effective thermal conductivity has little effect on the distribution of pressure and capillary force, i.e., the curvature of menisci, in the case of fixed heat flux. The effect of effective thermal conductivity on them is presented, respectively, in Figs. 6a and 7b at $q = 2000\ \text{W/m}^2$ and in Figs. 8a and 9b at $q = 20,000\ \text{W/m}^2$. The numerical results agree with the preceding prediction. As shown in Fig. 8a, profiles of pressure are fully superposed. Whereas in numerical simulation, we can see that the predicted phenomenon is more evident at higher heat fluxes than at lower heat fluxes.

Profiles of temperature with different effective thermal conductivity are presented in Fig. 6b at $q = 2000\ \text{W/m}^2$ and in Fig. 8b at $q = 20,000\ \text{W/m}^2$, respectively. The effective thermal conductivity does not change the ratio of energy in evaporation to heat in heating but influences strongly the spatial distribution of heat. And the effective thermal conductivity also influences the relation of heat conduction and convection. Figure 6b indicates that heat conduction of the porous structure is more important than convection of the working fluid, whereas Fig. 8b indicates the effect of convection is stronger than the effect of heat conduction or comparative to the

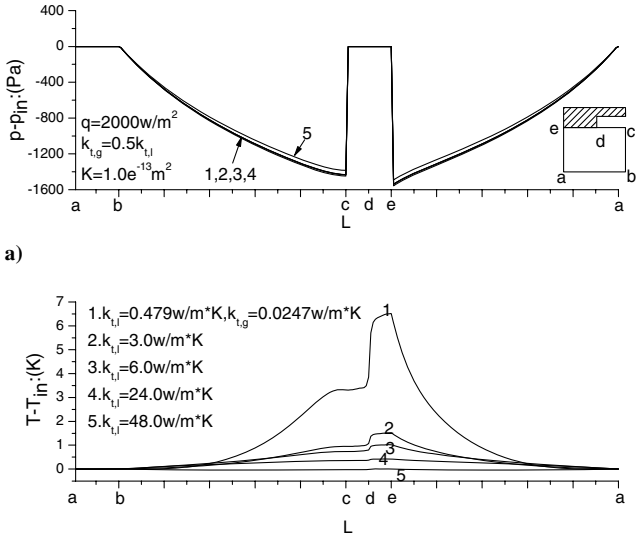

Fig. 6 Effect of effective thermal conductivity on a) pressure and b) temperature.

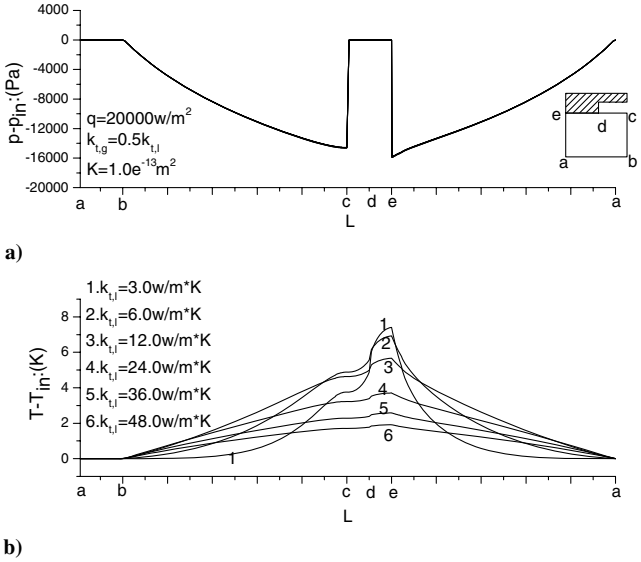

Fig. 8 Effect of effective thermal conductivity on a) pressure and b) temperature.

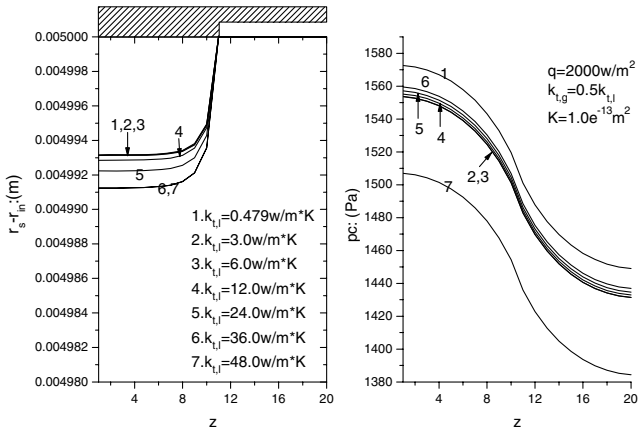

Fig. 7 Effect of effective thermal conductivity on a) position of the interface and b) capillary force.

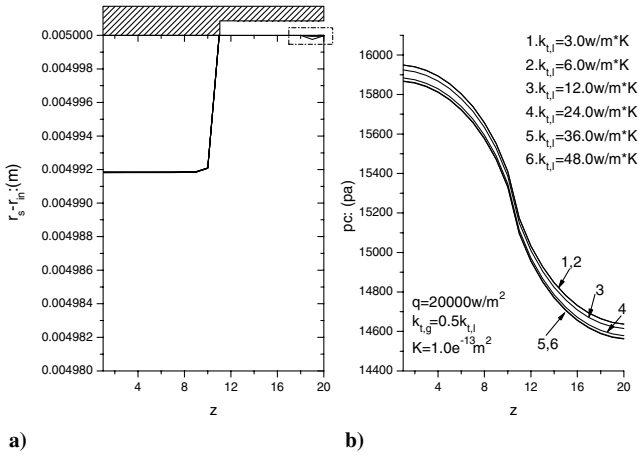

Fig. 9 Effect of effective thermal conductivity on a) the position of the interface and b) capillary force.

effect of heat conduction. By the results shown in Fig. 6b and 8b, we can obtain the following points. Higher effective thermal conductivity causes heat to be distributed homogeneously in each region and maintains a smaller temperature drop in the wick and less heat leak on the entrance, where the slope of the profile of temperature on the boundary a–b determines the heat leak there. Moderate effective thermal conductivity leads to a larger temperature drop everywhere and more heat leak on the entrance. Lower effective thermal conductivity leads to the convection of the working fluid that is more important than the heat conduction of the porous structure. Results of lower effective thermal conductivity are shown in profiles 1 and 2 of Fig. 8b; a high-temperature region exists on the top adjacent heated fins, and the bottom region maintains a low-temperature that reduces heat leak. As shown in segment c–d, there is a region of scarce heat support on the top far from the heated fins.

The effect of the effective thermal conductivity on the position of the interface is presented in Fig. 7a at $q = 2000\ \mathrm{W/m^2}$ and in Fig. 9a at $q = 20,000\ \mathrm{W/m^2}$. Profiles of the interface shown in Fig. 9a are fully superposed with different effective thermal conductivity, and those shown in Fig. 7a move a little as the effective thermal conductivity changes. According to the preceding discussion, there are three competing dynamic and thermodynamic processes: evaporation, heat conduction of the porous structure, and convection of the cool working liquid. At lower heat fluxes, such as $q = 2000\ \mathrm{W/m^2}$, the effect of heat conduction is more important than the effect of convection so that the behavior of the interface is a result of the competition between evaporation and heat conduction of the porous structure. Because heat is diffused homogeneously in the wick by heat conduction, the interface moves in far from the heated fin as the effective thermal conductive increases. At lower heat fluxes, the working fluid seems to "freeze" in the porous medium to be evaporated. Whereas at higher heat fluxes, such as $q = 20,000\ \mathrm{W/m^2}$, the effect of convection is comparative to the effect of heat conduction, or the process of convection is primary. The behavior of the interface is a result of the competition between evaporation and convection of the cool working liquid. The effective thermal conductivity has little effect on the position of the interface. Generally, the effective thermal conductivity of a liquid-saturated granule-packed or sintered porous media is lower than the maximum value given in our simulation, and the critical heat flux is higher than heat fluxes in our simulation. Thus, compared with heat conduction of the porous structure, convection of the cool working liquid is primary when a LHP works at the critical heat flux. Khrustalev and Faghri [11] pointed out that the critical heat flux was reached when the increase of the thermal resistance between the heated surface of the fin and the liquid zone with increasing heat flux lead to an extremely high temperature, which is unacceptable in practice, or when the thickness of the vapor zone around the fin is equal to the thickness of the porous structure. According to the preceding analysis, we can predict that the effective thermal conductivity has little effect on the heat transfer limit of LHPs.

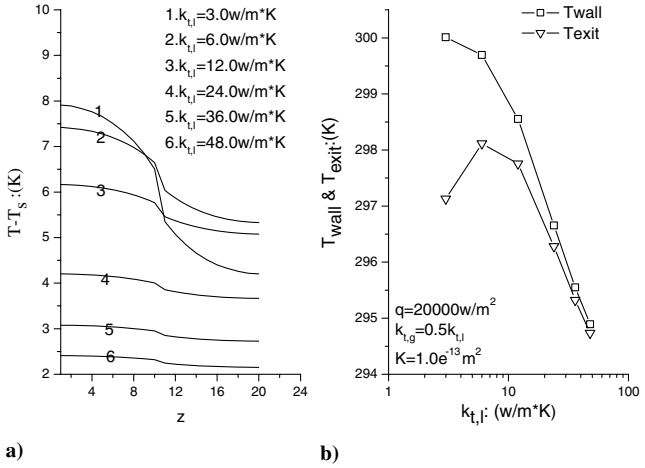

Fig. 10 Effect of effective thermal conductivity on a) interface superheating temperature $T - T_s$, b) mean temperatures T_{wall} and T_{exit}.

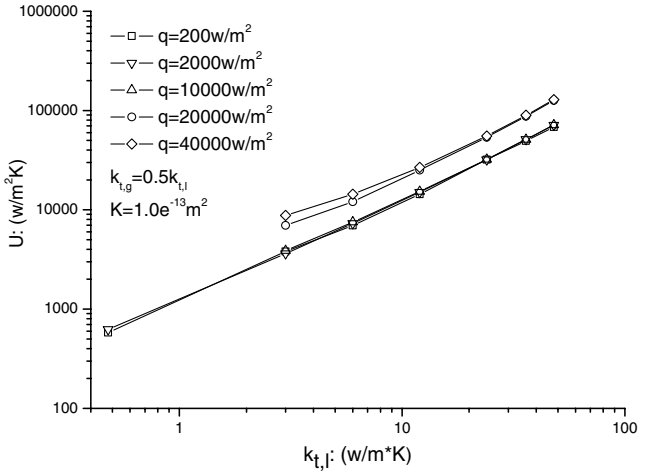

Fig. 11 Effect of effective thermal conductivity on the wick's total heat transfer coefficient in log–log coordinates.

The capillary force on the interface P_c, the superheating temperature on the interface $T - T_s$, the mean fin temperature T_{wall}, and the mean exit temperature T_{exit} with different effective thermal conductivity are presented in Figs. 7b, 9b, and 10. The closer the region is to the heated fin, the greater the capillary force is, which indicates that the working fluid is evaporating most strongly in the region closest to the center of heat source. The wick organizes evaporation more difficultly in the region closer to the center of heat source due to greater a superheating temperature shown in Fig. 10a. As shown in Figs. 10a and 10b, the superheating temperature on the interface and the mean fin temperature increase as the effective thermal conductivity decreases. The mean exit temperature increases to a peak and then decreases as the effective thermal conductivity decreases, which indicates that there lies a local low-temperature region in the vicinity of the grooves because low effective thermal conductivity leads to scarce heat support.

Finally, the effect of the effective thermal conductivity on the heat transfer efficiency is studied. The total heat transfer coefficient of the capillary wick is defined as the following:

$$U = \frac{q}{T_{\text{wall}} - T_{\text{exit}}} \tag{15}$$

The effect of the effective thermal conductivity on the coefficient is presented in Fig. 11, where a special case, $k_{t,l} = 0.247\ \text{W/m} \cdot \text{K}$, represents that the framework's thermal conductivity is equal to the liquid ammonia's thermal conductivity. Because the total heat transfer effect depends on evaporation, convection of the working fluid, and heat conduction of the porous structure, the coefficient U increases as the effective thermal conductivity increases. The relation of the total heat transfer coefficient versus the effective thermal conductivity is approximately linear in log–log coordinates, and it is presented by the following formula:

$$U = C(q) \cdot k_{t,l}^{\alpha} \qquad (q \leq 40{,}000\ \text{W/m}^2) \tag{16}$$

where $C(q)$ is a function of heat flux, which represents the contribution of convection to heat transfer in porous media, and α is constant with the value of 0.975–1.055. As shown in Fig. 11, the formula fits well when the effect of heat conduction is primary. And we can see that the total heat transfer coefficient increases exponentially when the effect of convection is primary.

By investigating the effect of the effective thermal conductivity on the wick's working state and performance, we conclude that the effective thermal conductivity has little effects on the wick's driving performance, and so it is feasible to focus on the wick's driving performance with no attention to others. Firstly, the research for the single object makes us apprehend deeply what affects the driving performance and how it is influenced, and it is easy to be realized. Secondly, those results that have been already been obtained in experiments or simulation of similar porous structures but using other materials with different thermal conductivity are used to describe the driving performance of these wicks.

Conclusions

An axisymmetric two-dimensional mathematical model of the cylindrical evaporator's wick of LHPs is developed to simulate heat transfer with flow and evaporation in the capillary porous structure. The effect of the interaction between the flowfield and the liquid–vapor interface on the position of the interface and the curvature of menisci is adequately considered in this model. The results obtained in this paper agree with the fact.

The wick's effective thermal conductivity has little influence on the driving performance but affects strongly the spatial distribution of heat in the porous structure. High effective thermal conductivity enhances total the heat transfer coefficient and eliminates heat leak to the liquid line.

Acknowledgements

The authors would like to acknowledge the support of the Chinese Academy of Space Technology. Thanks to Hu Mao-Bin for the discussion about this paper.

References

[1] Kaya, T., and Hoang, T. T., "Mathematical Modeling of Loop Heat Pipes and Experimental Validation," *Journal of Thermophysics and Heat Transfer*, Vol. 13, No. 3, 1999, pp. 314–320.

[2] Kaya, T., and Hoang, T. T., "Mathematical Modeling of Loop Heat Pipes with Two-Phase Pressure Drop," AIAA Paper 99-3448, 1999.

[3] Hoang, T., and Ku, J., "Hydrodynamic Aspects of Capillary Pumped Loops," Society of Automotive Engineers Paper 961435, 1996.

[4] Ku, J., "Operating Characteristics of Loop Heat Pipes," Society of Automotive Engineers Paper 1999-01-2007, 1999.

[5] Hoang, T., "Development of an Advanced Capillary Pumped Loop," Society of Automotive Engineers Paper 972325, 1997.

[6] Pouzet, E., Joly, J. L., Platel, V., Grandpeix, J. Y., and Butto, C., "Dynamic Response of a Capillary Pumped Loop Subjected to Various Heat Load Transients," *International Journal of Heat and Mass Transfer*, Vol. 47, No. 10–11, 2004, pp. 2239–2316.

[7] Vasiliev, L. L., "Heat Pipes in Modern Heat Exchanges," *Applied Thermal Engineering*, Vol. 25, No. 1, 2005, pp. 1–19.

[8] Maydanik, Yu. F., "Loop Heat Pipes," *Applied Thermal Engineering*, Vol. 25, Nos. 5–6, 2005, pp. 635–657.

[9] Zhang, H. X., Lin G. P., Ding, T., Yao, W., Shao, X. G., Sudalov, R. G., and Maidanik, Y. F., "Investigation of Startup Behaviors of a Loop Heat Pipe," *Journal of Thermophysics and Heat Transfer*, Vol. 19, No. 4, 2005, pp. 509–518.

[10] Tao, W. Q., *Neoteric Advance in Numerical Heat Transfer*, Science Press, Beijing, 2001, pp. 233–237, 283–286, (in Chinese).
[11] Khrustalev, D., and Faghri, A., "Heat Transfer in the Inverted Meniscus Type Evaporator at High Heat Fluxes," *International Journal of Heat and Mass Transfer*, Vol. 38, No. 16, 1995, pp. 3091–3101.
[12] Zhao, T. S., and Liao, Q., "On Capillary-Driven Flow and Phase-Change Heat Transfer in a Porous Structure Heated by a Finned Surface: Measurements and Modeling," *International Journal of Heat and Mass Transfer*, Vol. 43, No. 7, 2000, pp. 1141–1155.
[13] Demidov, A. S., and Yatsenko, E. S., "Investigation of Heat and Mass Transfer in the Evaporation Zone of a Heat Pipe Operating by the 'Inverted Meniscus' Principle," *International Journal of Heat and Mass Transfer*, Vol. 37, No. 14, 1994, pp. 2155–2163.
[14] Figus, C., Bray, Y. L., Bories, S., and Prat, M., "Heat and Mass Transfer with Phase Change in a Porous Structure Partially Heated: Continuum Model and Pore Network Simulation," *International Journal of Heat and Mass Transfer*, Vol. 42, No. 14, 1999, pp. 2557–2569.
[15] Takahashi, A. R., Oliveira, A. A., and Bazzo, E., "Analysis of Heat and Mass Transfer with Phase Change in the Porous Wick of a Capillary Pump," *Proceedings of the 7th International Heat Pipe Symposium*, Korean Society of Mechanical Engineers, Oct 2003, pp. 21–28.